On the Structure of the Inverse-Feasible Region of a Multiobjective Integer Program

Tyler Perini[a], Daniel Qiu[b], Silviya Valeva[c], Andrew J. Schaefer[d]

[a]*Department of Mathematics, United States Naval Academy, Annapolis, MD, USA*
[b]*Department of Industrial Systems Engineering, Seattle, WA, USA*
[c]*Department of Decision and System Sciences, Saint Joseph's University, Philadelphia, PA, USA*
[d]*Department of Computational Applied Mathematics and Operations Research, Rice University, Houston, TX, USA*

Abstract

Many optimization problems are made more challenging due to multiple, conflicting criteria. The subjective nature of balancing these criteria motivates techniques for inverse optimization. This study establishes foundations for an exact representation of the inverse feasible region of a multiobjective integer program. We provide the first insights into its exact structure, as well as two well-structured outer approximations to better capture its odd form. The first approximation is based on incomparability (where no solution should dominate another), and the second is based on supportedness (where some solutions should be optimal for a weighted sum scalarization). We include novel visualization tools to establish geometric intuition of the approximations' structure. We define several convexity-related subproblems, including convex cores and half-space coverings.

Keywords: multiobjective optimization, inverse optimization, integer programs

1. Introduction

The presence of multiple, conflicting objectives in an optimization problem complicates decision-making in many applications, such as healthcare [1, 2], engineering [3, 4], and more [5, 6, 7]. Whereas the goal of single-objective optimization is to return one optimal solution, in general no "ideal" solution exists for practical applications where all objectives are optimized simultaneously. Therefore, the common goal of multiobjective optimization is to compute *efficient solutions*, the set of which is the *efficient frontier* [5].

Intensity-modulated radiation therapy (IMRT) is a challenging multiobjective optimization problem [8]. Multiple treatment beams must be adjusted to target cancer cells while sparing nearby healthy tissues. The dosing model's parameters are unknown and depend on anatomy as well as tumor size and shape. IMRT requires balancing tumor irradiation and healthy tissue damage. A successful treatment plan may require multiple iterations, which is costly and time-consuming. However, historical data on optimized plans are readily available. Thus, estimating appropriate objective parameters based on prior successful treatment plans can establish standardized procedures while allowing a clinician to focus on minor plan adjustments. With wide-spread data availability, decision makers are often faced with the problem of making sense of *when* certain decisions are optimal. Situations like this motivate the study of inverse optimization.

While *forward optimization* seeks an optimal solution given an objective function and constraints, *inverse optimization* seeks model parameters under which a given solution becomes optimal or efficient. Methods typically infer either the objective or the constraint parameters. The focus of this work is to infer objective parameters for multiobjective integer linear programs (MOIPs). Previous analyses for inverse single objective linear [9] and integer [10] programs employed linear programming duality and superadditive duality, respectively. There are interesting relationships between the superadditive dual of a single-objective integer program and the efficient frontier of a (related) multiobjective integer program [11]. However, there are only nascent concepts available for a supperadditive dual of a MOIP [12]. This work establishes a different path toward an exact representation of the inverse feasible region by intersecting approximations of the set.

1.1. Literature and Applications

Inverse continuous optimization is well-studied. Early applications included geophysical studies [13], shortest paths [14], and more general network flow models [15]. Duality theory allows for an inverse linear problem to be formulated as a linear optimization problem itself. [15] use a target criteria vector and seek to find the minimum perturbation from that vector that would render a given set of feasible solutions optimal. Others, like [16] and [17], focus on recovering constraints for a linear program. Studies of inverse optimization beyond linear programs include conic and convex models

[18, 19, 20], Markov decision processes [21, 22], integer and mixed integer programs [23, 24, 10, 25]. See [26] for a recent and comprehensive review of the state of research, including applications, in single-objective inverse optimization.

Both the forward and inverse optimization problems are more challenging in the presence of multiple objectives. Inverse multiobjective optimization is more challenging as the goal is to find objective matrices that place all target solutions on the efficient frontier. For example, inverse multiobjective optimization may search for an objective matrix that achieves the target efficient frontier and that is nearest an initial objective matrix. One of the earliest inverse optimization studies was for IMRT [8]. [27, 28] and [29] formulate the dosing problem as an inverse optimization model with different aspects of treatment effects as the objectives and the laser treatment plans as the solutions. Inverse multiobjective linear programming [30] and combinatorial optimization [31] have been studied.

In the multiobjective literature, inverse optimization is closely related to the study of *weight space decompositions (WSDs)* [32, 33]. However, WSD is a more narrow analysis since it studies (i) a single weighted scalarization (typically weighted sum) and (ii) assumes fixed objectives and, as a result, only the the scalarization weight varies. In inverse optimization, the *entire* space of possible objectives is searched, which leads to higher-dimensional structures and requires additional theoretical machinery.

1.2. Contributions

This work contributes to the literature on global sensitivity analysis of mathematical programs [34], which acknowledges that the parameters defining the objectives, constraints, and bounds are subject to change. The work establishes an understanding of the inverse feasible region of a MOIP. Unlike the case of multiobjective linear programs, where convexity provides leverage, convexity is not available in this discrete setting. In order to compute the unsupported images, special techniques are required which result in convex-like properties; *e.g.*, "star-shaped" regions in WSD [33]. Our research identifies additional convex-adjacent subproblems, including convex cores and half-space covering.

Our main contributions can be summarized as:

- we present novel visualization strategies to observe the structure of the inverse feasible region of a MOIP;

- we develop two outer approximations of the inverse feasible region;
- we demonstrate examples and structural properties of each approximation; and
- we identify many open directions for future research.

The outline of the manuscript is as follows. Section 2 summarizes preliminary definitions, including the two major outer approximations studied. Sections 3 and 4 present analysis of the two outer approximations. Section 5 concludes with observations about the gap between the outer approximations and the inverse feasible set.

2. Preliminaries

For $p > 1$, let $y, z \in \mathbb{R}^p$. Isolated vectors are assumed to be column vectors, and for readability, we often omit transpose unless the dimension is not clear from context. Define the following (partial) vector orderings:

- $y < z$ if $z - y$ has all positive components;
- $y \leqq z$ if $z - y$ has all nonnegative components, where we say z *weakly dominates* y; and
- $y \leq z$ if $y \leqq z$ and $y \neq z$, where we say z *dominates* y.

Let $Y \subseteq \mathbb{R}^p$. A vector $y \in Y$ is *nondominated (ND)* with respect to Y if it is not dominated by a vector in Y. If y does not dominate z and vice versa, they are called *incomparable*, denoted by $y \sim z$. If all vectors in Y are pairwise incomparable, then Y is said to be *stable*. Note that the ND subset of any set is stable.

Let a multiobjective integer program (MOIP) have n integer decision variables, m constraints, and p objectives. We assume that constraints and objectives are defined by affine inequalities and linear functions, respectively, and henceforth we assume that the formulation is linear. For objective matrix $C \in \mathbb{R}^{p \times n}$ and $1 \leq i \leq p$, the ith row is denoted c^i and represents the vector for the ith objective. Vector $Cx \in \mathbb{R}^p$ is called the *image* of solution $x \in \mathbb{R}^n$. We consider MOIPs of the form

$$\mathrm{MOIP}(C) \coloneqq \mathrm{Max}\{Cx \mid Ax \leqq b, \quad x \in \mathbb{Z}^n_{\geqq}\},$$

where the "Max" operator returns the ND subset of images, the constraint matrix is $A \in \mathbb{R}^{m\times n}$, and the right-hand side vector is $b \in \mathbb{R}^m$.

The *(forward) feasible region*, $\mathcal{X} := \{x \in \mathbb{Z}^n_{\geqq} \mid Ax \leqq b\}$, exists within the *decision space*, $\mathbb{R}^n$. Throughout this work, we assume that A and b are fixed, and that $\mathcal{X}$ is nonempty and bounded. Let $C \in \mathbb{R}^{p\times n}$ be an objective matrix, and denote the *image set* by $\mathcal{Y} := C\mathcal{X} = \{Cx \mid x \in \mathcal{X}\}$, which exists in the *image space*, $\mathbb{R}^p$. Let $\bar{x} \in \mathcal{X}$ be a feasible solution and $\bar{y} := C\bar{x} \in \mathcal{Y}$ be its associated image. Image $\bar{y}$ is *(weakly) nondominated (ND)* if no other feasible image $y \in \mathcal{Y}$ (strictly) dominates it; in this case, $\bar{x}$ is called a *(weakly) efficient solution*. The set of efficient solutions is called the *efficient frontier*, denoted $\mathcal{X}_E(C)$, and the set of all ND images is called the *ND frontier*.

In the analysis of the ND set of a MOIP, the concept of the convex hull is critical to classifying solutions and images. A *scalarization* replaces a vector-valued objective function with a scalar-valued objective function. The most common scalarization, called the *weighted sum scalarization*, uses a positive (nonnegative and nonzero) weight vector $\lambda \in \mathbb{R}^p_{>}$ $(\mathbb{R}^p_{\geq})$ and is defined as:

$$\max\{\lambda^\top Cx \mid x \in \mathcal{X}\}. \tag{1}$$

If x^* is optimal for (1) with $\lambda \in \mathbb{R}^p_{>}$ $(\mathbb{R}^p_{\geq})$, then x^* is (weakly) efficient. Moreover, Cx^* lies on the (weakly) ND boundary of $\operatorname{conv}(\mathcal{Y})$. Hence, for $x^* \in \mathcal{X}_E(C)$, if there exists $\lambda \in \mathbb{R}^p_{\geq}$ such that x^* is optimal to the weighted sum scalarization, then the solution and its image are said to be *supported*; otherwise, they are *unsupported*. Let $\mathcal{X}_{SE}(C)$ denote the set of supported efficient solutions to MOIP(C). The relationship between convexity and this scalarization illustrates why analysis by this scalarization faces the same limitations as convex analysis. The challenge arises with the search for unsupported ND images that lie in the interior of $\operatorname{conv}(\mathcal{Y})$; this is especially important when the ratio of unsupported images in a ND set is nontrivial.

The (typical) *forward* MOIP is to solve for the efficient frontier given complete information, *i.e.*, fixed A, b, and C. However, the *inverse* problem we analyze here is: given A, b, and a target subset of feasible solutions, determine an explicit description for the *set of objective matrices* such that the target subset coincides with the efficient frontier. For instance, let $x^0 \in \mathcal{X}$. We say an objective matrix $C \in \mathbb{R}^{p\times n}$ is *inverse-feasible for solution* x^0 if $x^0 \in \mathcal{X}_E(C)$. More generally, we consider a set of solutions $\bar{X} := \{x^1, \ldots, x^s\} \subseteq \mathcal{X}$, where $s \geq 1$.

Definition 1. *An objective matrix* $C \in \mathbb{R}^{p\times n}$ *is said to be* inverse-feasible *for set* $\bar{X}$ *if* $\bar{X} = \mathcal{X}_E(C)$. *We define the* inverse-feasible region *as the set of objective matrices such that* $\bar{X}$ *is the efficient frontier of MOIP*(C), *denoted by*

$$D^*_E(\bar{X}) \coloneqq \{C \in \mathbb{R}^{p\times n} \mid \bar{X} = \mathcal{X}_E(C)\}.$$

A more strict representation of the inverse-feasible region, which will be more amenable to our analysis, is additionally conditioned on the target supported solutions, $\bar{X}_{SE} \subseteq \bar{X}$:

$$D^*_E(\bar{X}, \bar{X}_{SE}) \coloneqq \{C \in \mathbb{R}^{p\times n} \mid \bar{X} = \mathcal{X}_E(C) \text{ and } \bar{X}_{SE} = \mathcal{X}_{SE}(C)\}.$$

We introduce new labels for the space of (multi)objective matrices, $\mathbb{R}^{p\times n}$, as the *inverse-matrix space*, and the space of (single-)objective vectors, $\mathbb{R}^n$, as the *inverse-vector space*. While inverse-vector space coincides in dimension with decision space, they intuitively relate to very different concepts, and so the distinct labels will facilitate our presentation.

2.1. Inverse Feasible Regions for Single-Objective IPs

For the single-objective case (fixed $p = 1$), see [10] for a full analysis. We denote the single objective vector by $c \in \mathbb{R}^n$, and

$$\mathrm{IP}(c) \coloneqq \max\{cx \mid Ax \leqq b, \quad x \in \mathbb{Z}^n_{\geqq}\},$$

where $\mathrm{IP}(c)$ denotes the (scalar) optimal value. Two continuous relaxations of this discrete problem are important. First, the LP relaxation removes integrality constraints (replaces $x \in \mathbb{Z}^n_{\geqq}$ with $x \in \mathbb{R}^n_{\geqq}$), which in general does not yield a tight relaxation. Second, the convex hull relaxation replaces constraint set with $x \in \mathrm{conv}\{Ax \leqq b \mid x \in \mathbb{Z}^n_{\geqq}\}$ and is the tightest possible relaxation for single-objective IPs.

Definition 2. *Let* $\bar{x} \in \mathcal{X}$. *The inverse feasible region for the single-objective problem is denoted by*

$$D^*(\bar{x}) = \{c \in \mathbb{R}^n \mid c\bar{x} = IP(c)\}.$$

Note that the notation is without subscript and with a single solution as input. For any $\bar{x} \in \mathcal{X}$, $D^*(\bar{x})$ is always a polyhedral, pointed cone, including the case that $D^*(\bar{x}) = \{\vec{0}\}$. The boundaries of the $D^*(x)$ cones relate to the isoprofit objective vectors. Since these structures are central to our study, we provide the following fundamental definitions.

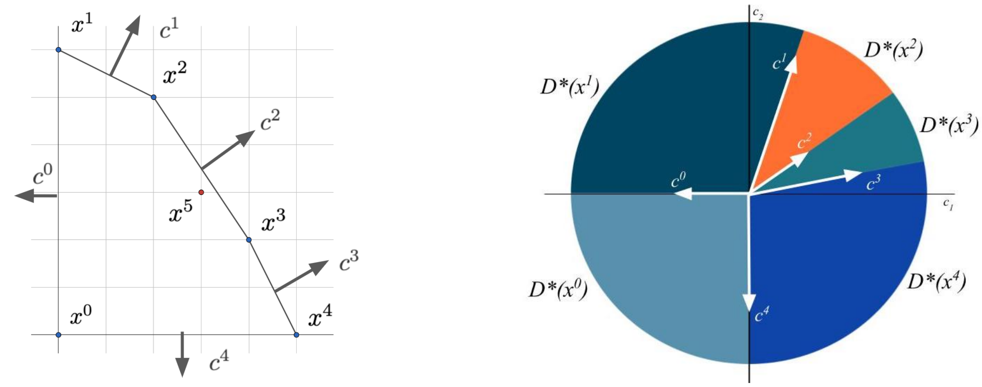

(a) (Forward) Feasible set illustrated in decision space.

(b) Single-objective inverse feasible sets, $D^*(x^i)$, illustrated in inverse-vector space.

Figure 1: Example 1.0 with isoprofit objective vectors.

Definition 3. *Nonzero* $c^* \in \mathbb{R}^n$ *is an* isoprofit objective vector *for* $x^1, x^2 \in \mathcal{X} \subset \mathbb{R}^n$ *if* x^1 *and* x^2 *are simultaneously optimal solutions to IP*(c^*)*. (This is not a unique vector.) As the name suggests, an isoprofit objective vector equally values two given solutions, and there exists* $d \in \mathbb{R}$ *such that* $c^*x^1 = c^*x^2 = d$*.*

2.2. Running Examples and Visualizations

The following running example is used to demonstrate concepts throughout the manuscript.

Example 1.0. *Let a discrete (forward) feasible set* $\mathcal{X} \subset \mathbb{Z}^2$ *be defined by the following linear constraints:*

$$\mathcal{X} \coloneqq \{x \in \mathbb{Z}^2_{\geqq} \mid x_1 + 2x_2 \leq 12, \quad 3x_1 + 2x_2 \leq 16, \quad 2x_1 + x_2 \leq 10\}.$$

See Figure 1a. The extreme points of the convex hull are labeled as: $x^0 = (0,0)$*,* $x^1 = (0,6)$*,* $x^2 = (2,5)$*,* $x^3 = (4,2)$*, and* $x^4 = (5,0)$*. Isoprofit objective vectors for adjacent extreme points are as follows:* $c^0 = [-1,0]$*,* $c^1 = [1,2]$*,* $c^2 = [3,2]$*,* $c^3 = [2,1]$*, and* $c^4 = [0,-1]$*. Solution* $x^5 = (3,3)$ *is noteworthy to distinguish between single-objective optimality and multiobjective efficiency: As it is not on the boundary of* $\text{conv}(\mathcal{X})$*, it is not optimal for any single objective including weighted sum scalarization. However, it still may be (unsupported) efficient for certain objectives (see Example 1.2).*

We use Example 1.0 to demonstrate the three visual representations recurring throughout the manuscript.

Decision space. Figure 1a is a traditional visualization technique representing the (forward) feasible set, $\mathcal{X}$, in decision space, $\mathbb{R}^2$.

Inverse-vector space. Figure 1b is a second visualization technique that represents inverse feasible objective vectors in inverse-vector space (also $\mathbb{R}^2$), where individual objectives can be shown. For simplicity, we choose to depict the inverse-feasible region as restricted to the unit disk, *i.e.*, vectors have a maximum Euclidean length of one.

Example 1.1. *In Figure 1b, the cones emanating from the origin, labeled as the inverse (single-objective) feasible set $D^*(x^i)$, denote the set of objective vectors for which x^i is optimal for the single-objective IP. In fact, the rays defined by isoprofit vectors c^0, c^1, c^2, c^3, and c^4 form the boundaries of the inverse feasible sets $D^*(x^0), \ldots, D^*(x^4)$. Note that $D^*(x^5) = \{\vec{0}\}$ (not labeled) since it is only optimal for the zero objective vector. Every solution in the interior of* $\mathrm{conv}(\mathcal{X})$ *is only optimal for the zero objective vector, i.e., there are no empty D^* cones.*

Visualization of decision space and inverse-vector space is limited to $n \leq 3$, but for demonstration purposes, we only include an example for $n = 2$. The inverse-vector space is useful for visualizing a single objective matrix comprised of multiple objective vectors, but it becomes limited when trying to visualize *multiple* objective matrices. Since the elements of the inverse-feasible region are many such matrices, this visualization is inadequate for more than a single feasible inverse-feasible solution. This motivates the following tool to overcome this challenge.

θ-space. For the particular case of two variables and two objectives ($n = p = 2$) and objective matrices with nonzero rows, we may use polar coordinate representation of each objective vector to achieve a 2-dimensional representation of all objective matrices. For each nonzero objective vector $c^i \in \mathbb{R}^2$ represented as (r^i, θ^i), magnitude r^i is immaterial and therefore omitted; only the angle θ^i matters. (The nonuniqueness of θ^i is addressed later.) Hence, this visualization technique, which we call *θ-space*, uses $\mathbb{R}^2$ to illustrate the (θ^i, θ^j) pairs representing the objective vectors for multiple biobjective matrices of the form $C = [c^1; c^2]$.

Remark 1. *That there do exist generalizations from polar coordinates to any $n > 2$. However, while spherical coordinates exist for 3-dimensional representations, i.e., the case of $n = 3$, this technique suffers from the many* *counterintuitive and computational challenges often faced in 3-dimensional visualization.*

Remark 2. *Zero objective vectors are excluded from our claims. The polar representation of zero vectors are undefined.*

Example 1.2. *Consider the following biobjective IP with the trivial identity objective matrix:*

$$\max_{x \in \mathcal{X}} \begin{pmatrix} 1 & 0 \\ 0 & 1 \end{pmatrix} x.$$

Note that the solution set, $\mathcal{X}$, is equivalent to the image set, $\mathcal{Y}$, and that x^5 is an efficient solution (ND image) here because no other integer feasible solution (image) dominates it. Therefore the complete efficient set for this biobjective IP is $\mathcal{X}_E = \{x^1, x^2, x^3, x^4, x^5\}$. The objective vectors, $c^1 = (1, 0)$ and $c^2 = (0, 1)$, could be visualized in the inverse-vector space, as in Figure 1b. These objective vectors have the polar representations $(1, 0)$ and $(1, \frac{\pi}{2})$, respectively. Therefore, the identity objective matrix $C = [c^1; c^2]$ is represented by coordinate pair $(\theta^1, \theta^2) = (0, \frac{\pi}{2})$. Similarly, the permuted objective matrix $C = [c^2; c^1]$ is represented by coordinate pair $(\theta^2, \theta^1) = (\frac{\pi}{2}, 0)$. Each matrix is represented as a single point in Figure 2a, and note the symmetry across the $\theta_2 = \theta_1$ line.

The objective vectors from Example 1.0 have the following polar representations, (r^i, θ^i): $(1, \pi)$, $(\sqrt{5}, \arctan 2)$, $(\sqrt{13}, \arctan \frac{2}{3})$, $(\sqrt{5}, \arctan \frac{1}{2})$, and $(1, \frac{3\pi}{2})$. Hereon the radii are omitted. Recall that a (nonzero) vector with polar angle θ is also equivalently represented by $\theta \pm 2\pi k$ for all $k \in \mathbb{Z}$. In our θ-space visualizations, this is observable as a continuation across the right-most edge and the left-most edge of the graph, and continuation across the top-most edge and the bottom-most edge (in "Pacman"-like fashion, see Figure 2b).

Figure 2b is a stylistic representation of our research questions for the inverse MOIP problem: What other objective matrices lead to the same efficient frontier? What are the shape and size of the inverse feasible regions? As a preview, observe Figures 2c and 2d which are simulated inverse feasible regions for Example 1.0. First, Figure 2c shows the inverse feasible regions when $\bar{X}$ is a singleton, i.e., $D_E^*(\{x^0\}), \ldots, D_E^*(\{x^4\})$. In θ-space, we can see that each of these regions is a simple square along the diagonal. The singleton case is the bridge between the single-objective perspective and our new multiobjective understanding. Second, Figure 2d shows more complex inverse

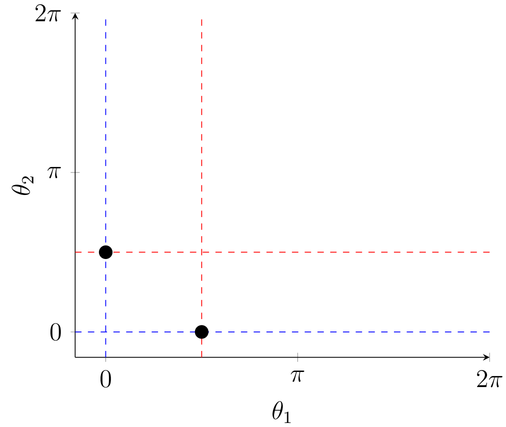

(a) θ-space representations of objective matrices $[1, 0; 0, 1]$ and $[0, 1; 1, 0]$.

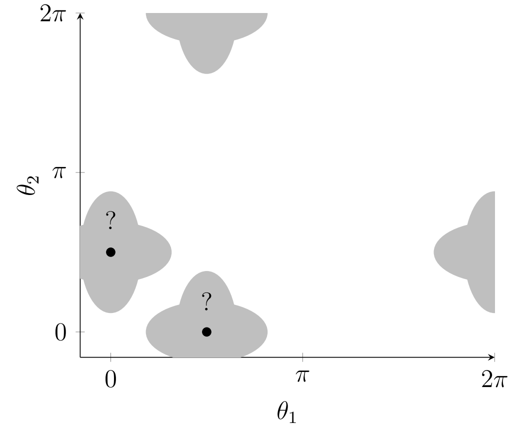

(b) The inverse optimization problem asks: what is the *shape and size* of the inverse feasible set, illustrated in gray?

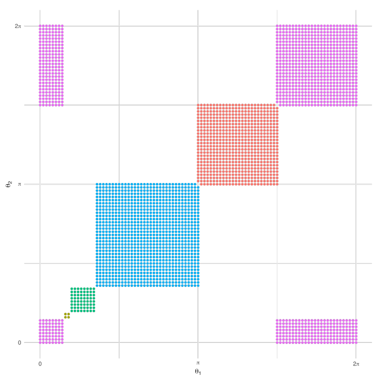

(c) A view of six inverse feasible sets (distinguished by color) when the efficient set is a singleton.

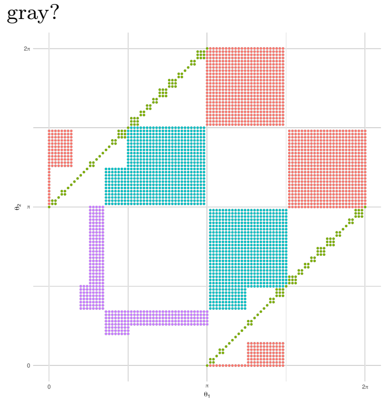

(d) A view of four inverse feasible sets (distinguished by color) for efficient sets of various size.

Figure 2: Illustrating the biobjective inverse optimization problem in θ-space. Note that θ-space visuals continue from the right edge to the left edge (and from the bottom edge to the top edge) due to the periodicity of polar angles. Plots (c) and (d) are computed by brute force grid search.

feasible regions when $\bar{X}$ has more than one solution. What follows is a better understanding of how to characterize and understand these structures.

2.3. Outer Approximations

Recall that $\bar{X} \subset \mathcal{X}$ is a given target set of solutions that should be efficient. Two relaxations for $D^*_E(\bar{X})$ are presented which are understood to

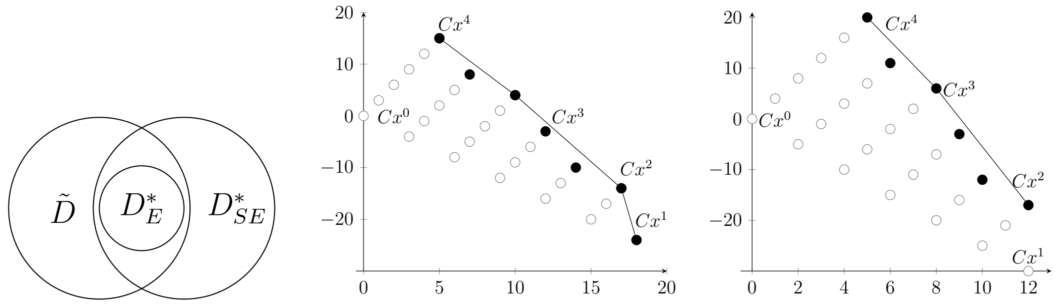

(a) For fixed sets $\bar{X}_{SE} \subseteq \bar{X}_E \subseteq \bar{X}$, the relationship between target set $D_E^*(\bar{X}_E)$ and outer approximations $\tilde{D}(\bar{X})$ and $D_{SE}^*(\bar{X}_{SE})$.

(b) The image set for biobjective matrix $C = [1, 3; 3, -4]$. Here, $C \in \tilde{D}(\bar{X}_E) \setminus D_{SE}^*(\bar{X}_E)$ since all target solutions are mutually incomparable, however the supported solutions do not match the target set $\bar{X}_{SE}$.

(c) The image set for biobjective matrix $C = [1, 2; 4, -5]$. Here, $C \in D_{SE}^*(\bar{X}_{SE}) \setminus \tilde{D}(\bar{X}_E)$ since all target solutions are supported, however x^1 is dominated, so $\bar{X}_E$ is not stable.

Figure 3: Representations of the outer approximation sets, including objective matrices not contained in D_E^*. For (b) and (c), the solution set is given in Example 1.0, the target efficient set is $\bar{X}_E = \{x^1, x^2, x^3, x^4\}$, and the target supported set $\bar{X}_{SE} = \{x^2, x^3, x^4\}$. ND images are darkened, and the supported images are outlined.

be nontight but are amenable to analysis. The first outer approximation is referred to as the *inverse supported set*, which is only conditioned on a target subset that should be supported, denoted $\bar{X}_{SE} \subseteq \bar{X}$. The inverse supported set is defined as

$$D_{SE}^*(\bar{X}_{SE}) \coloneqq \{C \in \mathbb{R}^{p \times n} \mid \bar{X}_{SE} = \mathcal{X}_{SE}(C)\}, \tag{2}$$

which is analogous to D_E^* except that $\mathcal{X}_E(C)$ is replaced by the supported counterpart $\mathcal{X}_{SE}(C)$. Importantly, set D_{SE}^* will always be simpler to analyze since a supported efficient solution is optimal to a single objective problem, and hence we may use analytical tools from single objective optimization. The second outer approximation, referred to as the *inverse incomparable set*, is defined as

$$\tilde{D}(\bar{X}) \coloneqq \{C \in \mathbb{R}^{p \times n} \mid C\bar{X} \text{ is stable}\}. \tag{3}$$

Sections 3 and 4 analyze these approximations, respectively.

Proposition 1 and Figure 3 summarize the subset relationship between the sets. What follows is more in-depth discussion of the more nuanced relationships between these sets.

Proposition 1. *Let $\bar{X} \subseteq \mathcal{X}$ such that $D^*_E(\bar{X})$ is nonempty. For some $C \in D^*_E(\bar{X})$, let $\bar{X}_{SE} = \mathcal{X}^*_{SE}(C)$. Then*

$$D^*_E(\bar{X}, \bar{X}_{SE}) \subseteq D^*_{SE}(\bar{X}_{SE}) \cap \tilde{D}(\bar{X}).$$

Proof. Suppose that $C \in D^*_E(\bar{X})$, and let $\mathcal{Y} = C\mathcal{X}$. Then every image in $C\bar{X}$ is ND with respect to $\mathcal{Y}$, which implies image set $C\bar{X}$ is stable. Thus, $C \in \tilde{D}(\bar{X})$. By assumption, there exists C such that $C\bar{X}_{SE}$ is the supported efficient subset of $\mathcal{Y}$. Since $C \in D^*_E(\bar{X})$ and $\bar{X}_{SE} = \mathcal{X}^*_{SE}(C)$, we trivially have $C \in D^*_{SE}(\bar{X}_{SE})$. □

Consider the following observations about the assumptions of Proposition 1. The given target set is $\bar{X}$, from which we assume the inverse problem is feasible and choose one inverse feasible objective matrix, C, to act as the "ground truth." Set $\bar{X}_{SE}$ is the supported efficient set for this ground truth objective matrix. It is understood that there could be multiple possible supported subsets, depending on the choice of C; however, this nuance is inconsequential to this study since we expect that $\bar{X}_{SE}$ will be given. Said another way, there is no uniqueness claim made in Proposition 1. For instance, given $\bar{X}$, neither C is the unique objective matrix for which $\bar{X}$ is the efficient set, nor $\bar{X}_{SE}$ is the unique supported set when $\bar{X}$ is efficient. In doing so, our proposition generalizes appropriately to all inverse feasible matrices, C. Additionally, when all efficient solutions are supported ($\bar{X}_{SE} = \bar{X}$), the following two sets coincide: $D^*_E(\bar{X}) = D^*_{SE}(\bar{X})$.

Note that a simple containment relationship between the sets $D^*_{SE}(\bar{X}_{SE})$ and $\tilde{D}(\bar{X})$ (in either direction) does not generalize; there are overlapping and disjoint portions, as demonstrated by Figure 3(b) and (c). Assume $\bar{X}_{SE} \subset \bar{X}_E \subset \bar{X}$. It may often be the case that there exists $C \in D^*_{SE}(\bar{X}_{SE}) \setminus \tilde{D}(\bar{X})$, which yields a dominated image in $C\bar{X} \setminus C\bar{X}_{SE}$. Similarly, there may often exist $C' \in \tilde{D}(\bar{X}) \setminus D^*_{SE}(\bar{X}_{SE})$, which yields a stable ND set but not the appropriate (un)supported images.

Example 1.3. *From the running example, let $\bar{X} = \bar{X}_{SE} = \{x^1, x^2\} = \{(0,6),(2,5)\}$. Figure 4 illustrates the important sets we study. Observe both subset relationships $D^*_E(\bar{X}) \subseteq D^*_{SE}(\bar{X}_{SE})$ and $D^*_E(\bar{X}) \subseteq \tilde{D}(\bar{X})$. For this instance, we have that $D^*_{SE}(\bar{X}_{SE}) \subset \tilde{D}(\bar{X})$, and so supportedness provide a tighter appoximation than stability. (This does not generalize.)*

2.3.1. Symmetry by Permutation

Our analyses are agnostic to the labeling of the objectives. For instance, when image set $C\bar{X}$ is stable for objective matrix $C = [c^1; \ldots; c^p]$, then the image set will remain stable for any permutation (relabeling) of these objectives. That is, the definitions of dominance and incomparability are *symmetric under permutation* of objective indices. Hence, the sets D^*_E, D^*_{SE}, and $\tilde{D}$ are all closed under permutation.

Proposition 2. *Let $\emptyset \subset \bar{X}_{SE} \subseteq \bar{X} \subseteq \mathcal{X}$ and $c^1, \ldots, c^p \in \mathbb{R}^n$. Objective matrix $[c^1; \ldots; c^p] \in D^*_E(\bar{X}, \bar{X}_{SE})$ if and only if $[c^{\sigma(1)}, \ldots, c^{\sigma(p)}] \in D^*_E(\bar{X}, \bar{X}_{SE})$ for all permutations $\sigma : \{1, \ldots, p\} \to \{1, \ldots, p\}$. The same is true for $D^*_{SE}(\bar{X}_{SE})$ and $\tilde{D}(\bar{X})$.*

Symmetry facilitates computation because certifying one element does (not) belong to a set implies certification of many more elements by permutation. This symmetric property can be observed in Figure 4 as symmetry over the line $\theta_2 = \theta_1$.

2.3.2. Trivial Objective Matrices

Consider that for the single objective problem with a zero objective vector (IP($\vec{0}$)), every feasible solution is optimal. Figure 1b makes this property clear as all cones intersect at the origin. In the multiobjective setting, a zero objective matrix maps every feasible solution to the origin, so the image set is trivially stable, and every feasible solution is efficient and supported.

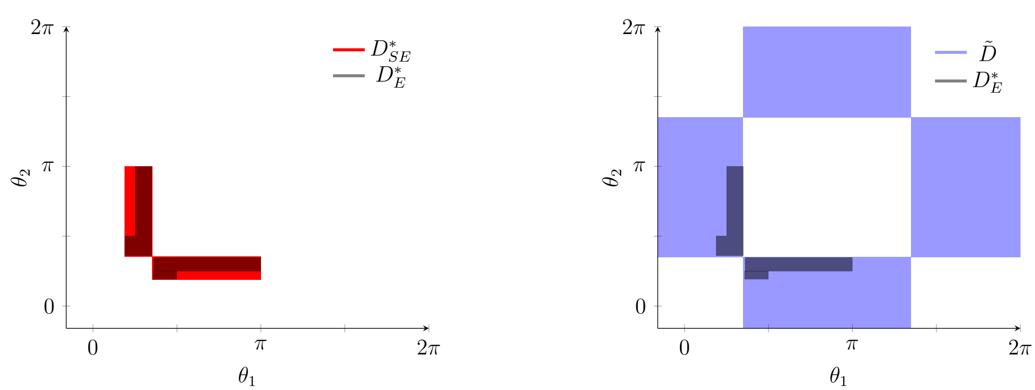

Figure 4: The target inverse feasible set, $D^*(\bar{X})$, is illustrated in θ-space, superimposed, as two dark gray, L-shaped regions. The outer approximation based on supportedness, $D^*_{SE}(\bar{X}_{SE})$, are two boxes in red. The outer approximation based on stability, $\tilde{D}(\bar{X}$ is illustrated in blue as a complex union of boxes.

Proposition 3. *The zero objective matrix is feasible to the inverse incomparable set, i.e.,* $0 \in \tilde{D}(\bar{X})$*, for any* $\emptyset \subset \bar{X} \subseteq \mathcal{X}$*. It is inverse feasible, i.e.,* $0 \in D^*_E(\bar{X}, \bar{X}_{SE})$*, if and only if* $\bar{X}_{SE} = \bar{X} = \mathcal{X}$*.*

Note that, unlike the single-objective case, the inverse MOIP feasible region may be empty. This is in part due to the strictness of the definition of $D^*_E(\bar{X}, \bar{X}_{SE})$.

2.3.3. Self-Conflicting Objective Matrices

A broader class of objective matrices is always feasible to the inverse incomparable set, $\tilde{D}(\bar{X})$.

Definition 4. *We say objectives* c^1 *and* c^2 perfectly conflict *(or are* perfectly conflicting*) if* $c^2 = -\alpha c^1$ *for some scalar* $\alpha > 0$*. An objective matrix* C *is said to be* self-collinear *if for every row* $j > 1$ *there exists nonzero* α^j *such that* $c^j = \alpha^j c^1$ *with at least one negative* α^j*.*

This property is stronger than having row rank of one. For example, let $c \in \mathbb{R}^n \setminus \{0\}$ be fixed. Then $C = [c; 2c; 3c; 4c]$ is not self-collinear by our definition (even though every row vector belongs to one line), but $C' = [c; -2c; 3c; 4c]$ satisfies our definition due to the negative second row. Self-collinear objective matrices are not inherently practical or insightful for most applications. However, they are always feasible to the outer approximation $\tilde{D}$. We prove this for the biobjective case which generalizes to $p > 2$.

Proposition 4. *For any* $\bar{X} \subseteq \mathcal{X}$ *and self-collinear objective matrix* C*,* $C\bar{X}$ *is stable.*

Proof. The cases $|\bar{X}| = 0$ and $|\bar{X}| = 1$ are trivial. We prove the claim for $|\bar{X}| > 1$ and $p = 2$. Let the self-collinear objective matrix be $C = [c^1, -\alpha c^1]$ for $\alpha > 0$, and let x^1, $x^2 \in \bar{X}$ be distinct. We denote the associated images as $y^1 = (c^1 x^1, -\alpha c^1 x^1)$ and $y^2 = (c^1 x^2, -\alpha c^1 x^2)$. We have 3 cases: (i) If $c^1 x^1 = c^1 x^2$, then the second components also coincide, $-\alpha c^1 x^1 = -\alpha c^1 x^2$, and therefore $y^1 = y^2$ and so $y^1 \sim y^2$. (ii) If $c^1 x^1 < c^1 x^2$, then $-\alpha c^1 x^1 > -\alpha c^1 x^2$. They are again incomparable. The remaining case (iii) follows from the reverse argument for (ii). Since x^1 and x^2 are chosen arbitrarily, we can conclude that all elements of $\bar{X}$ are pair-wise incomparable, and hence it is a stable set. Furthermore, the image set belongs to a line, *i.e.*, $C\bar{X} \subset \{y \in \mathbb{R}^2 | y_2 = -\alpha y_1\}$, such that every image is efficient and supported. These arguments generalize to $p \geq 3$. $\square$

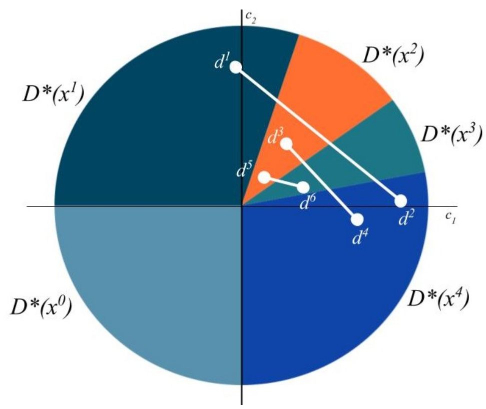

Figure 5: Inverse-vector space for Example 1.0. Objective vectors are illustrated by points. For a biobjective matrix with two objective vectors, the line segment indicates the objectives possible via weighted sum scalarization.

3. Properties of Inverse Supported Set

We have defined the inverse feasible set, $D^*_E(\bar{X}, \bar{X}_{SE})$, as a function of two input sets: $\bar{X}$ is the target set of efficient solutions and $\bar{X}_{SE}$ is the target set of supported solutions. It is most practical to assume that $\emptyset \subset \bar{X}_{SE} \subset \bar{X} \subset \mathcal{X}$, with all subsets being strict. However, in the special case that $\bar{X}_{SE} = \bar{X}$ (*i.e.*, there are no unsupported solutions), then we have that $D^*_E(\bar{X}_{SE}, \bar{X}_{SE})$ reduces equivalently to the inverse supported set $D^*_{SE}(\bar{X}_{SE})$. This special case can be almost entirely understood through means of single-objective methods, *i.e.*, weighted sum scalarization. Therefore, this is a natural starting point. We begin by developing a geometric intuition for the inverse supported set in an incremental way.

Consider the biobjective case with two variables ($n = p = 2$). Suppose an objective matrix $D \in \mathbb{R}^{2\times 2}$ is inverse-feasible. Then both objectives d^1 and d^2 can be illustrated in inverse-vector space as individual points. The challenge for visualization becomes how to indicate that these two points should be treated as a single matrix. In Figure 5, we choose to link the two points by a line segment. For instance, $D = [d^1; d^2]$ is the first objective matrix, $D' = [d^3; d^4]$ is a second, and $D'' = [d^5; d^6]$ is a third. This strategy is only sufficient for visualizing a few objective matrices, since the figure becomes increasingly dense as the number of matrices increases.

This visualization provides an additional interpretation: For $D = [d^1; d^2]$, the line segment linking d^1 and d^2 is the set of *convex combinations* of these two objective vectors. Hence, it equivalently represents *all possible weighted sum scalarization* objectives (with respect to d^1, d^2, and nonnegative weights). We can use this intuition to identify which solutions are then supported for a fixed pair of objectives: every cone $D^*(x^i)$ intersected by the line segment is a supported solution in the efficient frontier.

Example 1.4. *Let $D = [d^1; d^2]$. The line segment in Figure 5 depicts the convex hull,* $\text{conv}\{d^1, d^2\}$*, and has nonempty intersection with $D^*(x^i)$ for $i = 1, 2, 3, 4$. Hence, for objective matrix D, $X_{SE} = \{x^1, x^2, x^3, x^4\}$. Similarly, for objective matrix $D' = [d^3; d^4]$, $X_{SE} = \{x^2, x^3, x^4\}$. Finally, for objective matrix $D'' = [d^5; d^6]$, $X_{SE} = \{x^2, x^3\}$.* $\square$

In the same way, an objective matrix for $p \geq 3$ could be represented by the convex hull of p objective vectors. The following result states the general equivalence between convex combinations of objective vectors and the inverse feasibility of D^*_{SE}. The key link is that supportedness is defined by the weighted sum scalarization, and the convex hull in inverse vector space captures all possible nonnegative weights.

Lemma 1. *Given $\mathcal{X}$ and $C \in \mathbb{R}^{p \times n}$, the supported efficient set $X_{SE}(C)$ each solution x with a cone $D^*(x)$ that intersects the interior of* $\text{conv}(c^1, \ldots, c^p)$*. That is,*

$$X_{SE}(C) = \{x \in \mathcal{X} \mid D^*(x) \cap \text{int}(\text{conv}(c^1, \ldots, c^p)) \neq \emptyset\}.$$

The interior of the convex hull excludes boundary cases that would lead to weakly efficient solutions, which are dominated. Lemma 1 implies some intuitive corollaries. First, if the zero objective vector is a convex combination of objectives, then every solution is supported. This relates to when a solution is only optimal for the zero objective vector, which can only be supported if this condition is met.

Corollary 1. *If $0 \in \text{int}(\text{conv}(c^1, \ldots, c^p))$, then $X_{SE}(C) = \mathcal{X}$. If $x \in \bar{X}_{SE}$ and $D^*(x) = \{\vec{0}\}$, then either $\bar{X}_{SE} = \mathcal{X}$ or $D^*_{SE}(\bar{X}, \bar{X}_{SE}) = \emptyset$.*

Corollary 1 is naturally limited in scope, especially with respect to binary integer programs where every feasible solution is an extreme point of $\text{conv}(\mathcal{X})$. Therefore, $D^*(x)$ is nonsingleton for every feasible $x \in \mathcal{X}$, and so Corollary 1 is never applicable. Although, a certificate of infeasibility is useful, since certifying an outer approximation, D^*_{SE}, as infeasible guarantees the inverse feasible set, D^*_E, is infeasible.

A second corollary relates to the *ideal point*, which is the image defined component-wise as the optimal value for every objective, *i.e.*, $y_i^I := \max\{c^i x \mid x \in \mathcal{X}\}$ for $i = 1, \dots, p$. When the ideal point is a feasible image, the ND frontier is just the singleton $\{y^I\}$. It is commonplace in multiobjective contexts to assume that the ideal point is infeasible. In our context, a similar case is associated with having a singleton target set, *i.e.*, $|\bar{X}| = 1$. The following claim identifies that this is when the multiobjective inverse feasible set reduces to the single-objective inverse feasible set.

Corollary 2. *If $\bar{X} = \bar{X}_{SE} = \{\bar{x}\}$, then C is inverse feasible if and only if $c^i \in D^*(\bar{x})$ for all $1 \le i \le p$. Equivalently, $D_E^*(\bar{X}, \bar{X}_{SE}) = D^*(\bar{x}) \times \cdots \times D^*(\bar{x}) = [D^*(\bar{x})]^p$.*

Next, we consider more complex cases. We are interested in whether the union of cones $\cup_{x \in \bar{X}_{SE}} D^*(x)$ remains convex or not. Since each individual cone is convex, there are just two cases of nonconvexity. The first is the case of non-pointed cones, *i.e.*, those that contain a line. (For example, in Figure 5, $D^*(x^0) \cup D^*(x^1) \cup D^*(x^4)$ is nonconvex.) This case is reasonable to address by an assumption, which is motivated by an application where we assume that the target set of supported solutions is possible to achieve. We interpret this to mean that the target supported set coexists on one region of the boundary of the feasible set. The assumption translates this geometric understanding to the inverse vector space.

Assumption 1. *We assume that for given $\bar{X}_{SE}$ that there exists a pointed cone P in inverse-vector space such that $D^*(x) \subset P$ for all $x \in \bar{X}_{SE}$.*

The following proposition provides the most general result. The proof is omitted.

Proposition 5. *Let $\bar{X}_{SE} \subset \bar{X}_E \subset \mathcal{X}$, $p \ge 2$ be fixed, and $c^1, \dots, c^p \in \mathbb{R}^n$ be nonzero such that $C := [c^1; \dots; c^p]$ is non-collinear. If $D^*(x) \cap \mathrm{int}(\mathrm{conv}(c^1, \dots, c^p))$ is nonempty for all $x \in \bar{X}_{SE}$ and empty for all $x \notin \bar{X}_{SE}$, then $C \in D_{SE}^*(\bar{X}_{SE})$*

.

The following example illustrates Proposition 5.

Example 1.5. *Given $\bar{X}_{SE} = \{x^2, x^4\}$ and $p = 2$, $D^*(x^2) \cup D^*(x^4)$ is nonconvex (see Figure 6a). There does not exist an objective matrix which makes x^2 and x^4 supported without x^3 also being supported. Given $\bar{X}_{SE} = \{x^2, x^3, x^4\}$,*

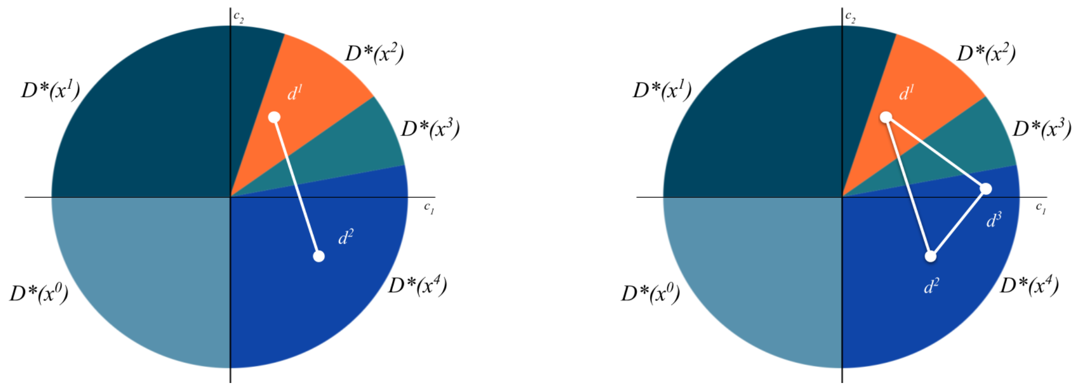

(a) (b)

Figure 6: Example 1.5, illustrating Proposition 5.

$D^*(x^2) \cup D^*(x^3) \cup D^*(x^4)$ is convex (see Figure 6b). For $p = 2$, $D := [d^1; d^2] \in D^*_{SE}(\bar{X}_{SE})$. For $p = 3$, we may also choose d^3 so that the convex hull of the vectors intersect only the desired cones; hence, $D' := [d^1; d^2; d^3] \in D^*_{SE}(\bar{X}_{SE})$.

The following are intuitive corollaries of Proposition 5. First is an existence result for the nice case of a convex union of cones.

Corollary 3. *Let $\bar{X}_{SE} \subset \bar{X}_E \subset \bar{X}$, and suppose $\cup_{x \in \bar{X}_{SE}} D^*(x)$ is a pointed, convex cone. Then for some finite $p \geq 2$, $D^*_{SE}(\bar{X}_{SE})$ contains an objective matrix that is not self-collinear.*

For one construction of an inverse feasible objective matrix, consider intersecting the union of cones with an affine hyperplane to represent normalizing, *e.g.*, $\{c \in \mathbb{R}^n \mid \sum_{i=1}^n c_i = 1\}$. Then some number of the extreme points of the polytope generate an objective matrix feasible to the inverse supported set. By this construction, p is the number of extreme points, which may be quite large. The second corollary provides that increasing the value of p will maintain feasibility.

Corollary 4. *If $D^*_{SE}(\bar{X}_{SE})$ is nonempty for $\bar{p} \geq 2$, then $D^*_{SE}(\bar{X}_{SE})$ is nonempty for all $p \geq \bar{p}$.*

Intuitively, since $\bar{p}$ objective vectors construct a sufficiently large convex hull, then choosing additional objective vectors (*e.g.*, within the convex hull) will obviously satisfy the conditions of Proposition 5, as well. Corollary 4 suggests that there is some minimal number of objectives, p^*, for which $D^*(\bar{X}_{SE})$ is nonempty, which we also consider subsequently.

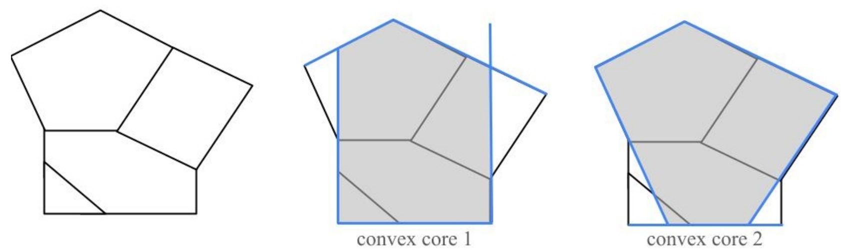

Figure 7: (Left) A family of convex polytopes, $\mathcal{F}$, whose union Π is nonconvex. (Middle) One convex core (in gray) which is representable by a subset of the constraints (in blue). (Right) A second convex core (in gray) which is representable by a subset of the constraints (in blue). Both convex cores have five extreme points and four extreme polyhedra.

3.1. Convex Core

Suppose we have that $\cup_{x \in \bar{X}_{SE}} D^*(x)$ is a union of cones that is pointed but nonconvex. This is not possible for two-dimensional space but possible for dimensions greater than two. We would like to inscribe $D^*_{SE}(\bar{X}_{SE})$ as a convex set confined within this nonconvex set. Therefore, as an alternative to the commonplace convex hull (*i.e.*, the smallest convex superset), we are interested in *maximal convex subset* contained within a set. This concept is natural in the context of nonconvex, self-intersecting polytopes. (For instance, the convex core of a small stellated dodecahedron is a dodecahedron.) Additionally, we require the subset to intersect all component sets. Given set Π, we define such a set to be a *convex core* of Π. Unfortunately, in our setting, there is no guarantee that Π has a single, unique convex core. Thus, we more broadly define the *set* of convex cores.

Definition 5 (Convex core)**.** *Let $\mathcal{F}$ be a family of polyhedra in $\mathbb{R}^n$, and let $\Pi = \cup_{P \in \mathcal{F}} P$ denote their union. A* convex core *of Π is a convex subset of Π which intersects every $P \in \mathcal{F}$ and is maximal with respect to subset inclusion. That is, there does not exist a convex set $S \subseteq \Pi$ such that S intersects every $P \in \mathcal{F}$ and core$(\Pi) \subset S$. The set of all convex cores is denoted by core(Π).*

See Figure 7 to illustrate a simple family of two-dimensional polyhedra with a nonconvex union and two distinct convex cores. If $\Pi = \cup_{P \in \mathcal{F}} P$ happens to be convex on its own, then it is trivial that it has a *unique* convex core (Π, itself). For the purposes of this manuscript, we do not explore additional conditions under which a family has a unique core or multiple cores.

For our study, we are interested in the family $\mathcal{F} = \{D^*(x)\}_{x \in \bar{X}_{SE}}$ with a nonconvex union, Π. The introduction of convex cores permits a more accurate description of D^*_{SE}. We are unaware of a practical representation or computational method for the convex cores of a general family of polytopes in the literature. For now, we present an approximate outline by means of eliminating constraints from the outer descriptions of the polyhedra.

Proposition 6 (Constraint Subset). *For $\mathcal{F} = \{P^1, P^2, \dots, P^k\}$ and $1 \le i \le k$, let $\Pi := \cup_{1 \le i \le k} P^i$. Assume each polytope has an inequality description in the form of $P^i := \{x \in \mathbb{R}^n \mid A^i x \le b^i\}$.*

1. *If $Q \in core(\Pi)$ is a convex core of Π, then $Q = \{x \in \mathbb{R}^n \mid A^Q x \le b^Q\}$ where every constraint $A^Q x \le b^Q$ belongs to (at least) one of the systems $A^i x \le b^i$ for $1 \le i \le k$.*
2. *If $a^\top x \le b$ is a constraint for P^i and $a^\top x \ge b$ is a constraint for P^j where $i \ne j$, then neither constraint are in an outer description for any convex core.*
3. *If $a^\top x \le b$ is a constraint for P^i and is valid for every polyhedron in the family, then $a^\top x \le b$ is a (possibly redundant) constraint for every convex core of Π.*

In short, Proposition 6 states that every convex core of Π may be represented as a subset of all the constraints used to represent $P^1, \dots, P^k$. In the following, we motivate the consequences of these structures.

The extreme points of a convex core are informative, as is the case for most convex sets. In our case, we use the extreme points of a convex core to label polyhedra in the family as *extreme*.

Definition 6 (Extreme Polyhedra). *Let $\mathcal{F}$ be a family of polyhedra in $\mathbb{R}^n$ and $\Pi(\mathcal{F}) = \cup_{P \in \mathcal{F}} P$. For $P \in \mathcal{F}$, P is called* extreme *with respect to Π if there exists some extreme point of a convex core(Π) in P. That is, if $Q \in core(\Pi)$ and $ext(Q) \in P$, then P is extreme.*

Suppose there is a unique convex core for Π. Then, we can directly infer the importance of every extreme polyhedra. Namely, the extreme polyhedra must be captured or "covered" by the choice of objective vectors. Moreover, as the number of extreme polyhedra increases, then the number of objective vectors required to "cover" the necessary D^* cones also increases.

Proposition 7 (Covering Extreme Polyhedra)**.** *Let $\mathcal{F}$ represent the family of polyhedra for the intersections of $D^*(x) \cap H$ for every $x \in \bar{X}_{SE}$ and some affine hyperplane H. Denote $\Pi = \cup_{P \in \mathcal{F}} P$. Suppose there is a unique convex core, denoted core$(\Pi) = \{Q\}$, and let κ be the number of extreme polyhedra. Then $D^*_{SE}(\bar{X})$ is feasible for $p \geq \kappa$.*

In the case that there is no unique convex core for Π, then the extreme polyhedra with respect to one core might differ (substantially) from the extreme polyhedra with respect to another core. Many research questions remain open.

3.2. Special Properties for Unit Lattice

In this section, we focus on the following example which is commonly encountered when working with binary decision variables. It is useful for generalizing to higher-dimensions while maintaining a simple structure.

Example 2.0. *Consider for $n \geq 2$ the lattice of n unit vectors and the origin, denoted by*

$$\Delta^n \coloneqq \left\{ x \in \{0,1\}^n \;\middle|\; \sum_{i=1}^{n} x_i \leq 1,\ x_i \geq 0 \quad \forall i = 1, \dots, n \right\}.$$

The following facts will be relevant: every $x \in \Delta^n$ is an extreme point of conv(Δ^n)*. Therefore, $D^*(x)$ is a nonsingleton for every $x \in \Delta^n$. The cones may be represented in closed form as*

$$D^*(\vec{0}) = \{d \in \mathbb{R}^n | d_j \leq 0 \quad \forall j = 1, \dots, n\} \quad \textit{and} \quad D^*(\vec{e_i}) = \{d \in \mathbb{R}^n | d_i \geq 0, d_i \geq d_j \quad \forall j \neq i\},$$

where $1 \leq i \leq n$ and $\vec{e_i}$ is the ith unit vector. Furthermore, every pair of feasible solutions of conv(Δ^n) *are adjacent by an edge. Hence, $D^*(x^1) \cap D^*(x^2)$ is nonempty for every distinct $x^1, x^2 \in \Delta^n$.*

Recall that Corollary 4 implies a minimum value of p exists such that $D^*_{SE}(\bar{X}_{SE})$ is nonempty. Specifically for Δ^n, Lemma 2 shows that any subset of the lattice is possible to be supported efficient for even the most restrictive case of $p = 2$. We denote $\{\bar{X}_{SE}, \bar{X}_U\} \subset \Delta^n$ as a nonempty partition of Δ^n, where $\bar{X}_U$ denotes the set of solutions to be either unsupported efficient or non-efficient.

Lemma 2. *Let $\{\bar{X}_{SE}, \bar{X}_U\} \subset \Delta^n$ be a nonempty partition of Δ^n. Then for $p = 2$, $D^*_{SE}(\bar{X}_{SE})$ is nonempty.*

The proof applies the observation that for objective matrix $C \in \mathbb{R}^{p\times n}$, the image set $C\Delta^n$ trivially yields n images equal to the columns of C and additionally the origin. Therefore, any desired image set with n images is attainable by constructing C. We view this simplified optimization problem as an *image selection* problem.

Proof. Let $p \geq 2$, $n \geq 3$, and $\Delta^n = \{x^0, x^1, \ldots, x^n\} \subset \{0,1\}^n$, where x^0 denotes the origin, and for $1 \leq i \leq n$, x^i denotes the feasible lattice point whose ith coordinate is 1 (remaining coordinates are 0). To simplify this proof, we assume $x^0 \notin \bar{X}_{SE}$, which may be handled with uninteresting modifications. without loss of generality, we assume $\bar{X}_{SE} = \{x^1, \ldots, x^s\}$ for $1 < s \leq n$ (any other solution set follows by permutation). We omit the trivial case where $s = 1$ (see Corollary 2). Recall that both objectives are maximized.

Note that for fixed n, p, s, there exists many frontiers which contain s supported ND images, which may either be constructed randomly or recursively. For such a ND image set, $\tilde{Y}$, let $\{y^1, y^2, \ldots, y^s\}$ be the subset of supported ND images. Use these images to construct the objective coefficients, where all components after the sth are zero, *i.e.*, define

$$c^1 = (y^1_1, y^2_1, \ldots, y^s_1, \vec{0}) \quad \text{and} \quad c^2 = (y^1_2, y^2_2, \ldots, y^s_2, \vec{0})$$

Let $C := [c^1; c^2]$. If $x^i \notin \bar{X}_{SE}$ for $1 \leq i \leq n$, then C maps x^i to the origin. Thus we have $C\Delta^n$ has image set $\{y^1, y^2, \ldots, y^s, \vec{0}\}$. Hence, solutions $x^1, \ldots, x^s$ are supported efficient, as desired. □

4. Properties of Inverse Incomparable Set

Whereas supportedness translates directly from single-objective optimization (via weighted sum scalarization), stability is a property unique to multiobjective optimization. Every efficient set is stable, but not vice versa. Figure 8 illustrates inverse incomparable sets in θ-space; note that the limits on the θ_1-axis are shifted (compared to other figures) for reasons discussed in Section 4.1.

The first property is that increasing the number of solutions in $\bar{X}$ decreases the region $\tilde{D}(\bar{X})$, which is formalized in Proposition 8.

Proposition 8. *If $\bar{X}^1 \subset \bar{X}^2 \subseteq \mathcal{X}$, then $\tilde{D}(\bar{X}^2) \subseteq \tilde{D}(\bar{X}^1)$.*

Example 1.6. *For $\bar{X}^1 = \{x^1, x^2, x^3\}$ and $\bar{X}^2 = \{x^1, x^2, x^3, x^4\}$, $\tilde{D}(\bar{X}^1)$ and $\tilde{D}(\bar{X}^2)$ are shown in Figure 8a, colored blue and red, respectively. Observe*

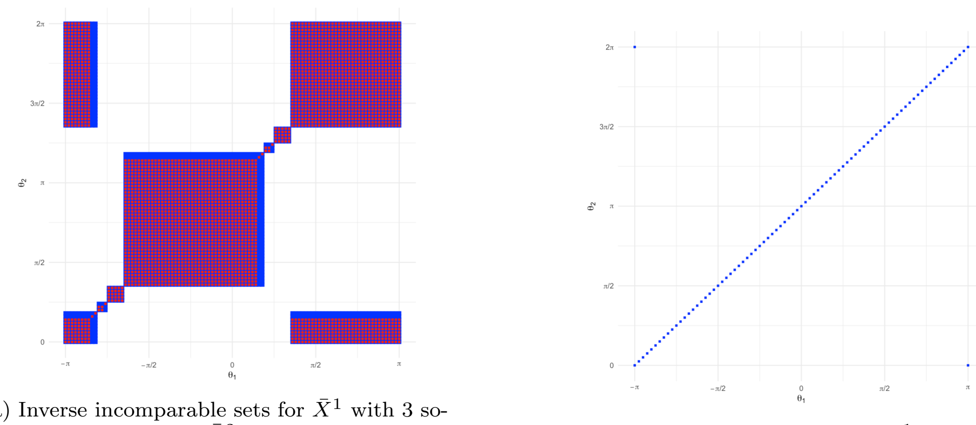

(a) Inverse incomparable sets for $\bar{X}^1$ with 3 solutions (in blue) and $\bar{X}^2$ with 4 solutions (in red).

(b) Inverse incomparable sets for $\{x^1, \ldots, x^{100}\}$ uniformly drawn from $x^i \in [0,1] \times [0,1]$.

Figure 8: Inverse incomparable sets ($\tilde{D}$) in θ-space for various solution sets $\bar{X}$. Note that the θ_1-axis has been shifted to the range $[-\pi, +\pi]$ (as opposed to $[0, 2\pi]$ in other figures) to highlight the antiparallel symmetry.

that $\tilde{D}(\bar{X}^2) \subseteq \tilde{D}(\bar{X}^1)$, i.e., the inverse incomparable region shrinks when introducing an additional solution. $\square$

4.1. Antiparallel Symmetry

Recall that Proposition 4 provides that $\tilde{D}(\bar{X})$ is nonempty for any $\bar{X} \subseteq \mathcal{X}$ since all self-collinear objective matrices are elements. By definition of self-collinear, the objective vectors satisfy $c^2 = -\alpha c^1$ for positive α, so the vectors are anti-parallel with π-radians between. Hence, in θ-space, the self-collinear objective matrices appear along the diagonal $\theta_2 = \theta_1 + \pi$ (or $\theta_2 = \theta_1 - \pi$) line. This line can be nicely observed in Figure 2d (in green). As $\bar{X}$ grows in size, and $\tilde{D}(\bar{X})$ reduces in size to just this diagonal line.

Example 1.7. *Figure 8b shows the inverse incomparable region for 100 points randomly selected from the unit square $[0,1] \times [0,1]$. Note that $\mathcal{X}$ need not be well-defined here for $\tilde{D}(\bar{X})$ to be simulated by brute force. The region $\tilde{D}(\bar{X})$ has been reduced to the diagonal line $\theta_2 = \theta_1 \pm \pi$, e.g., where the corresponding objective vectors may be $c_1 = -c_2$.*

Recall the line of symmetry by permutation, $\theta_2 = \theta_1$, discussed in Section 2.3.1. The line of self-collinear matrices provides an additional type of symmetry for $\tilde{D}$ which does not appear for D^*_{SE} or D^*_E. Both symmetries may be observed in Figure 8, where the $\theta_2 = \theta \pm \pi$ line appears in the set $\tilde{D}$ and the $\theta_2 = \theta_1$ line occurs in white space outside of the set. This anti-parallel symmetry may be interpreted as symmetry across the "nearest" self-collinear objective matrix.

Proposition 9. *Let $n = p = 2$. When viewed from θ-space, $\tilde{D}(\bar{X})$ is symmetric across line $\theta_2 = \theta_1$ and across lines $\theta_2 = \theta_1 \pm \pi$.*

4.2. Projection to θ-space

For every set $\bar{X} \subseteq \mathcal{X}$, region $\tilde{D}(\bar{X})$ is a union of polyhedral cones in inverse-matrix space emanating from the origin. For $n = p = 2$, this conic structure is amenable to the θ-space representation, wherein a two-dimensional rectangular region in θ-space denotes a cone with four facets in inverse-matrix space. In this biobjective setting, we work with pairs of objective vectors. Therefore, we clarify the structure of the Cartesian product of inverse feasible regions and projection to θ-space.

Proposition 10. *Let $P^1, P^2 \subset \mathbb{R}^2$ be pointed cones in inverse-vector space emanating from the origin defined by*

$$P^i := \{c \in \mathbb{R}^2 \mid c = (r\cos\theta, r\sin\theta), \quad \alpha_i \le \theta \le \beta_i, \quad r \ge 0\}$$

for some $\alpha_1, \alpha_2, \beta_1, \beta_2 \in \mathbb{R}$ such that $\alpha_i < \beta_i$ for $i = 1, 2$. Now $Q := P^1 \times P^2 \subset \mathbb{R}^{2\times 2}$ is a set of matrices in inverse-matrix space. The projection of Q to θ-space is $[\alpha_1, \beta_1] \times [\alpha_2, \beta_2] \subset \mathbb{R}^2$, which is rectangular with sides parallel to both axes and nonempty interior.

Example 1.8. *In Figure 8a, $\tilde{D}(\bar{X}^1)$ is the union of 6 pointed cones, indicated by six blue boxes, where one box continues across the both axes of θ-space. Similarly, $\tilde{D}(\bar{X}^2)$ is the union of seven cones strictly contained within $\tilde{D}(\bar{X}^1)$, represented by the seven red boxes.*

For the exhaustive method of computing the precise θ-space representation of $\tilde{D}$, which may offer further intuition, see the online supplement.

4.3. Half-Space Covering

Theorem 1 provides a general result for a structural description of $\tilde{D}(\bar{X})$. We use the notation $\operatorname{sign}(A) = -\operatorname{sign}(B)$ to indicate that $A > 0$ and $B < 0$ or vice versa.

Theorem 1. *Let* $\bar{X} = \{x^1, \ldots, x^s\} \subset \mathcal{X} \subset \mathbb{R}^n$ *and* $C = [c^1; \ldots; c^p]$ *for* $c^1, \ldots, c^p \in \mathbb{R}^n$. *Suppose for every distinct pair of solutions* $x^i, x^j \in \bar{X}$ *there exists* $q, r \in \{1, \ldots, p\}$ *such that*

$$\operatorname{sign}(c^q(x^i - x^j)) = -\operatorname{sign}(c^r(x^i - x^j)).$$

Then $C\bar{X}$ *is stable and* $C \in \tilde{D}(\bar{X})$.

Proof. Assume $n \geq 2, s \geq 2$, and $p \geq 2$. Let $\bar{X}$ and C be as given, and suppose for contradiction that $C\bar{X}$ is not stable. Then there exists $x, x' \in \bar{X}$ such that Cx dominates Cx', *i.e.*, $Cx \geqq Cx'$. So for $i \in \{1, \ldots, p\}$, $c^i x \geq c^i x'$ with at least one inequality strict. Equivalently, $c^i(x - x') \geq 0$ for all $i \in \{1, \ldots, p\}$, which contradicts the assumption that there exists q and r such that $c^q(x - x') > 0$ and $c^r(x - x') < 0$ (or vice versa). $\square$

The online supplement presents many useful examples of Theorem 1 for the reader to build intuition from small values of n, s, and p. In short, Theorem 1 expresses a half-space covering condition which, when satisfied, achieves the target supported efficient set. Finite n represents the dimension of inverse-vector space (and decision space). The number of solutions, s, determines the number of hyperplanes/half-spaces in the subdivision of the inverse-vector space. Finally, p determines the number of objective vectors to be selected to achieve the covering.

5. Conclusions

What has so far been presented are two outer approximations for D_E^*. Although not an exact representation, we believe together they form a close approximation. We denote the *characterization gap* of this approximation by

$$\Gamma(\bar{X}, \bar{X}_{SE}) \coloneqq D_{SE}^*(\bar{X}_{SE}) \cap \tilde{D}(\bar{X}) - D_E^*(\bar{X}, \bar{X}_{SE}).$$

The gap may be nonempty when $\bar{X}_{SE} \subset \bar{X} \subset \mathcal{X}$ (both subsets strict) and depends on the dominated solutions and unsupported efficient solutions. The online supplement includes the proof that the gap is nonempty with an example.

This work has established fundamental structures for inverse optimization of MOIP by extending ideas from single objective optimization and augmenting with concepts unique to multiobjective optimization. Two outer approximations were developed for the the target inverse feasible set, D_E^*.

First, supported images, characterized via single-objective optimization and viewed through the lens of convex combinations, led to the inverse supported set, D^*_{SE}. Second, the multiobjective notion of incomparable solutions led to the inverse incomparable set, $\tilde{D}$. We demonstrated examples of each outer approximation and important structural properties, including convex-adjacent properties, which would be pertinent to computational approaches. Lastly, we describe the known characterization gap between the target set and intersection of two outer approximations. Much remains to be explored in future research for reducing this gap with novel outer approximations, delving into the convex-adjacent properties, and implementing these insights into computational algorithms.

6. Acknowledgments

This research was supported by Office of Naval Research (N00014-21-1-2262). The views expressed in this article are those of the author(s) and do not reflect the official policy or position of the U.S. Naval Academy, Department of the Navy, the Department of Defense, or the U.S. Government.

Appendix A. Exact $\boldsymbol{\theta}$-Space Representation of $\tilde{\boldsymbol{D}}$

For an exact representation of $\tilde{D}(\bar{X})$, use set difference to remove the objective matrices which would yield one solution in $\bar{X}$ dominating another. Consider one single pair of solutions, $x^1, x^2 \in \bar{X}$. First, define region $R(x^1, x^2)$ to contain all the objective matrices C where x^1 weakly dominates x^2, *i.e.*, $C(x^1 - x^2) \geqq 0$. Define $\sigma^+ = x^1 - x^2$ and let θ^+ be the angle such that $\sigma^+ = [||\sigma^+|| \cos\theta^+, ||\sigma^+|| \sin\theta^+]$. We aim to capture $R(x^1, x^2)$ as a box in the form of $[a, b] \times [c, d]$, and note that this may exceed across border lines. Now we have

$$C = \begin{bmatrix} ||c^1|| \cos\theta^1 & ||c^1|| \sin\theta^1 \\ ||c^2|| \cos\theta^2 & ||c^2|| \sin\theta^2 \end{bmatrix}.$$

Then

$$\begin{aligned} 0 \leqq C\sigma^+ &= [||c^1|| \cdots ||\sigma^+||(\cos\theta^+ \cos\theta^1 + \sin\theta^+ \sin\theta^1), \quad ||c^2|| \cdots ||\sigma^+||(\cos\theta^+ \cos\theta^2 + \sin\theta^+ \sin\theta^2)] \\ &= [||c^1|| \cdots ||\sigma^+|| \cos(\theta^+ - \theta^1), \quad ||c^2|| \cdots ||\sigma^+|| \cos(\theta^+ - \theta^2)] \end{aligned}$$

Therefore, $\cos(\theta^+ - \theta^1) \geq 0$, and $\cos(\theta^+ - \theta^2) \geq 0$. So we infer ranges $\theta^1, \theta^2 \in [\theta^+ - \pi/2, \theta^+ + \pi/2]$. Equivalently, we have $R(x^1, x^2) = [\theta^+ - \pi/2, \theta^+ + \pi/2] \times [\theta^+ - \pi/2, \theta^+ + \pi/2]$ with center point (θ^+, θ^+).

Similarly, to compute $R(x^2, x^1)$, we need $C(x^2 - x^1) \geqq 0$, which implies $C\sigma^+ \leqq 0$. Note that we are still using $\sigma^+ = x^1 - x^2$ as before, so now θ^+ will no longer be the centerpoint. By similar computations we can conclude that $R(x^2, x^1) = [\theta^+ + \pi/2, \theta^+ + 3\pi/2] \times [\theta^+ + \pi/2, \theta^+ + 3\pi/2]$, which is centered at $(\theta^+ + \pi, \theta^+ + \pi)$. As a result, the closed form θ-space representation of $\tilde{D}(\{x^1, x^2\})$ is

$$\tilde{D}(\{x^1, x^2\}) \coloneqq \Theta - R(x^1, x^2) - R(x^2, x^1). \tag{A.1}$$

This aligns with our observation that the $\tilde{D}$ is symmetric along the line $\theta_2 = \theta_1 + \pi$.

Finally, we can represent the entire stable set $\tilde{D}(\bar{X})$ by using set difference over all possible pairs of solutions, *i.e.*,

$$\tilde{D}(\bar{X}) = \Theta - \bigcup_{x^1, x^2 \in \bar{X}} R(x^1, x^2).$$

The time complexity of the above method is $O(s^2)$.

Example 1.9. *Consider $\bar{X} = \{x^1, x^2\}$. Compute $\sigma^+ = [-2, 1]$, with $\theta^+ \approx 2.67$. The following sets can be observed in Figure A.9: The first box, $R(x^1, x^2)$, represents the set of objective matrices where x^1 dominates x^2 (outlined with solid lines), and is centered at (θ^+, θ^+). Note that this box is illustrated as white space, and that it continues past the vertical $\theta = \pi$ line and continues across the vertical $\theta = -\pi$ line. The second box, $R(x^2, x^1)$, represents the set of objective matrices where x^2 dominates x^1 (outlined with dashed lines), and is centered at $(\theta^+ - \pi, \theta^+ + \pi)$. Note that this box continues past the horizontal $\theta = 2\pi$ line and continues across the horizontal $\theta = 0$ line. Then the incomparability set, $\tilde{D}(\bar{X})$, is the blue region that remains after set subtraction of $R(x^1, x^2)$ and $R(x^2, x^1)$. Of course, for this simple case, we can infer the rectangular representation for $\tilde{D}(\bar{X})$ as the union of two rectangles (in blue):*

$$[\theta^+ - \tfrac{3\pi}{2}, \theta^+ - \tfrac{\pi}{2}] \times [\theta^+ - \tfrac{\pi}{2}, \theta^+ + \tfrac{\pi}{2}] \quad \cup \quad [\theta^+ - \tfrac{\pi}{2}, \theta^+ + \tfrac{\pi}{2}] \times [\theta^+ + \tfrac{\pi}{2}, \theta^+ + \tfrac{3\pi}{2}].$$

Appendix B. Theorem 1 Examples

We present several foundational cases of Theorem 1. First, consider the simplest case of $n = p = s = 2$. Observe that in order to be incomparable, one

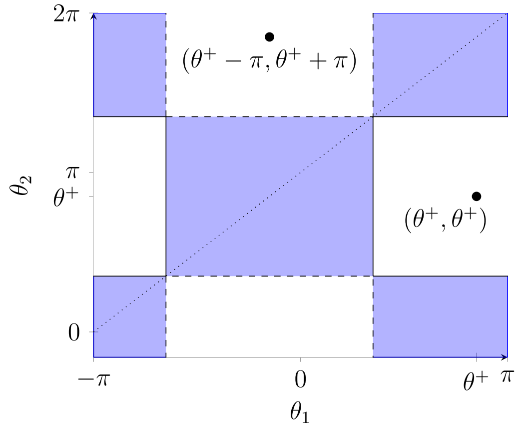

Figure A.9: Revisiting the running example for $\bar{X} = \{x^1, x^2\}$, which first appeared in Figure 4. The line of symmetry, $\theta_2 = \theta_1 \pm \pi$, is dotted. Note that the θ_1-axis has been shifted to the range $[-\pi, +\pi]$ (as opposed to $[0, 2\pi]$ in other figures).

objective must value x^1 over x^2 (*e.g.*, $c^1x^1 > c^1x^2$), and the other objective must value x^2 over x^1 (*e.g.*, $c^2x^1 < c^2x^2$). For sake of readability, we state the corollary for this special case.

Corollary 5. *($n = 2, s = 2, p \geq 2$) Let $\bar{X} = \{x^1, x^2\} \subset \mathcal{X} \subset \mathbb{R}^2$ and $C = [c^1; \ldots; c^p]$ for $c^1, \ldots, c^p \in \mathbb{R}^2$. If there exist $i, j \in \{1, \ldots, p\}$ such that $c^i(x^1 - x^2) > 0$ and $c^j(x^1 - x^2) < 0$, then $Cx^1 \sim Cx^2$ and $C \in \tilde{D}(\bar{X})$.*

Example 3 ($n = 2, s = 2, p = 2$)**.** *If $c^1(x^1 - x^2) > 0$ and $c^2(x^1 - x^2) < 0$, then $Cx^1 \sim Cx^2$ and $C \in \tilde{D}(\bar{X})$. The claim may be summarized geometrically with respect to the line spanned in inverse-vector space by the isoprofit objective vector; see Figure B.10. Consider c^1 as the isoprofit objective vector for x^1 and x^2. In inverse-vector space, the line spanned by c^1 contains the origin and extends infinitely in both directions. Let $D = [d^1; d^2]$ be an objective matrix. If d^1 and d^2 exist on opposite sides of the line, then the images of $\bar{X}$ are incomparable.*

We interpret Corollary 5 geometrically again with respect to Figure B.10: let c^* denote the isoprofit objective vector for two solutions x^1 and x^2. In order to provide incomparable images, objective matrix $[d^1; \ldots; d^p]$ must have at least one vector on each side of the line spanned by c^*. Hence, isoprofit vector c^* defines a subdivision into two half-spaces, and what remains is a

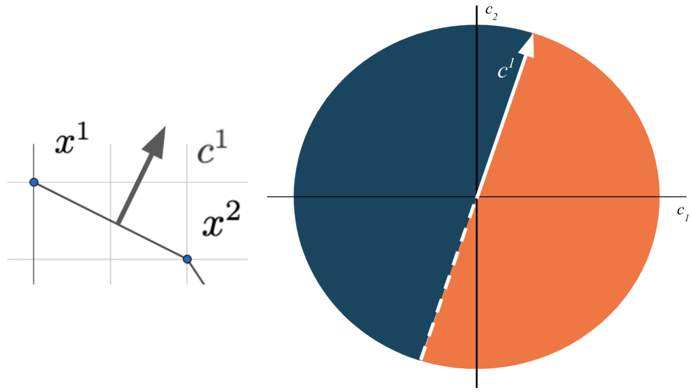

Figure B.10: (Left) For $\bar{X} = \{x^1, x^2\}$, c^1 is the isoprofit objective vector defined by the two solutions. (Right) The line spanned by c^1 bisects inverse-vector space into two half-spaces. For $p = 2$, objective matrix $[d^1; d^2]$ yields incomparable images if the vectors d^1 and d^2 belong to (the interior of) opposite half-spaces. For $p > 2$, objective matrix $[d^1; \ldots; d^p]$ yields incomparable images if there exist vectors d^i and d^j belonging to (the interior of) opposite half-spaces.

half-space covering problem where there are multiple ways to choose vectors d^i and d^j such that at least one vector is in one half-space (*i.e.*, $d^i(x^1 - x^2) < 0$) and at least one other vector is in the opposite half-space (*i.e.*, $d^j(x^1 - x^2) > 0$). A more natural interpretation of the mathematical condition $\text{sign}(d^i(x^1 - x^2)) = -\text{sign}(d^j(x^1 - x^2))$ is that it indicates when d^i and d^j cover opposite halfspaces with respect to the isoprofit vector for x^1 and x^2. The next special case considers more than two solutions, where we encounter more interesting half-space covering with an increasing number of half-spaces.

Example 4 ($s \geq 2$)**.** *Let $\bar{X} = \{x^1, x^2, x^3\}$ and $C = [c^1; c^2]$ for $c^1, c^2 \in \mathbb{R}^2$. Theorem 1 may be restated as: If for all distinct $i, j \in \{1, \ldots, s\}$ $sign(c^1(x^i - x^j)) = -sign(c^2(x^i - x^j))$, then $C\bar{X}$ is stable and $C \in \tilde{D}(\bar{X})$. There are three isoprofit objective vectors to consider: one for each pair of solutions. See Figure B.11a. Each isoprofit objective vector subdivides inverse-vector space into two half-spaces for a total of six half-spaces. Note that the focus is on individual half-spaces rather than the intersection of half-spaces.*

Figure B.11b illustrates a successful covering (left) and an unsuccessful covering (right). In the left subfigure, with respect to the darkened line, objective vector d^1 covers the blue halfspace, and objective vector d^2 covers the orange halfspace. By checking all six halfspaces, one can confirm that each

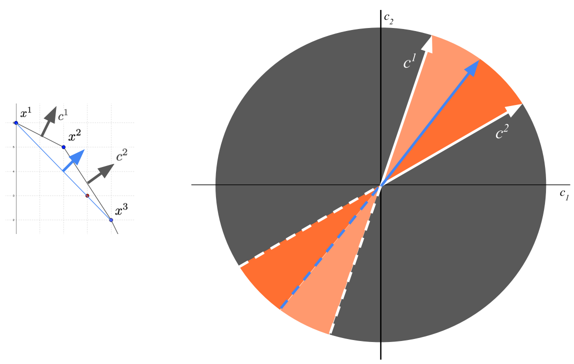

(a) Taken pairwise, the $s = 3$ solutions define three isoprofit objective vectors: c^1, c^2, and the third in blue. The line spanned by each objective vector divides the inverse-vector space into two half-spaces for a total of six half-spaces.

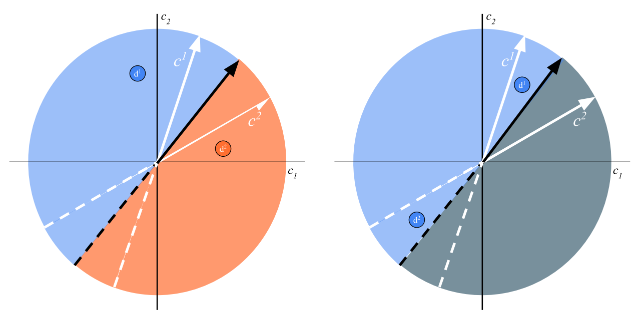

(b) On the left, the black line separates the blue halfspace, covered by d^1, and the orange half-space, covered by d^2. In fact, all six halfspaces are covered by d^1 and/or d^2. Note that the narrow cones are covered by multiple halfspaces. On the right, both objective vectors cover the blue halfspace, but neither objective vector covers the gray halfspace.

Figure B.11: Half-space covering conditions for $s > 2$ solutions.

halfspaces is covered by d^1 *or* d^2*. In the right subfigure, with respect to the darkened line, both objective vectors cover the same blue halfspace. Hence, the gray halfspace is uncovered. Intuitively, both* d^1 *and* d^2 *value* x^1 *over* x^3*, and so* x^1 *dominates* x^3*.*

Consider the following insights from Example 4: First, the lines (or hyperplanes for $k > 2$) through the origin subdivide the inverse-vector space into cones, which all emanate from the origin and only intersect at their boundaries. In order to guarantee that all halfspaces are covered for $p = 2$, the pair of chosen objective vectors must belong to *opposing* cones. That is, if P is one cone emanating from the origin as a result of the subdivision, then choosing $d^1 \in P$ and $d^2 \in -P$ will cover all half-spaces and hence result in a stable image set. In the left subfigure of Figure B.11b, we have chosen the objective vectors from opposing cones (the two widest cones). Hence, Theorem 1 provides a stronger sufficient condition than self-collinearity for choosing objectives which make a set of solutions stable.

Example 5 ($p \geq 2$)**.** *Consider selecting more than two objectives, e.g., choosing a third objective vector from the right subfigure of Figure B.11b. Since the only uncovered halfspace is the gray one, if objective vector d^3 were chosen from anywhere in the gray halfspace, then $D = [d^1; d^2; d^3]$ would yield a stable image set. As p increases, there are certainly many more configurations for $d^1, \ldots, d^p$ which feasibly cover all half-spaces.*

Example 6 ($n \geq 2$)**.** *Finally, consider cases where $n > 2$. For the geometric interpretation in higher-dimensional solution spaces, we address the nonuniqueness of isoprofit objective vectors for a given pair of solutions. Let $x^i, x^j \in \mathbb{R}^n$ be distinct solutions. Let $H(i,j) \coloneqq \{c^* \in \mathbb{R}^n | x^i \text{ and } x^j \text{ optimal for } IP(c^*)\}$ be the set of all isoprofit objective vectors, which is a subset of the hyperplane $\{c \in \mathbb{R}^n : c(x^i - x^j) = 0\}$ uniquely defined by its orthogonal vector $x^i - x^j$. This linear hyperplane is the generalization of the line spanned by c^* in the $\mathbb{R}^2$ case. Now, objective vectors are to cover both half-spaces defined by the linear hyperplane $H(i,j)$.*

Altogether, Theorem 1 expresses a half-space covering set that achieves the target supported efficient set. Finite n represents the dimension of inverse-vector space (and decision space). The number of solutions, s, determines the number of hyperplanes/half-spaces in the subdivision of the inverse-vector space. Finally, p determines the number of objective vectors to be selected to achieve the covering.

Appendix C. Characterization Gap for D_E^*

This section outlines the known *characterization gap* of the proposed approximation, denoted as

$$\Gamma(\bar{X}, \bar{X}_{SE}) \coloneqq D^*_{SE}(\bar{X}_{SE}) \cap \tilde{D}(\bar{X}) - D^*_E(\bar{X}, \bar{X}_{SE}).$$

The gap may be nonempty when $\bar{X}_{SE} \subset \bar{X} \subset \mathcal{X}$ (both subsets strict) and depends on the dominated solutions and unsupported efficient solutions. We prove the gap exists as a proposition, followed by an example.

Proposition 11. *Let $\emptyset \subset \bar{X}_{SE} \subset \bar{X} \subset \mathcal{X}$ be fixed. The characterization gap between $D^*_{SE}(\bar{X}_{SE}) \cap \tilde{D}(\bar{X})$ and $D^*_E(\bar{X}, \bar{X}_{SE})$ If the characterization gap $\Gamma(\bar{X}, \bar{X}_{SE})$ is nonempty, then each element $C \in \Gamma(\bar{X}, \bar{X}_{SE})$ yields one of the two following cases:*

- *a target unsupported efficient solution ($x \in \bar{X} - \bar{X}_{SE}$) is dominated, or*
- *a target dominated solution ($x \in \mathcal{X} - \bar{X}$) is efficient but unsupported.*

Proof. Suppose $C \in \tilde{D}(\bar{X}) \cap D^*_{SE}(\bar{X}_{SE})$. Denote $Y = C\bar{X}$, $Y_{SE} = C\bar{X}_{SE}$, and $Y_{bd} = \text{bound}(Y)$, i.e., the boundary of the convex hull of images. Then Y is guaranteed to be stable, and for $\bar{X}_{SE} \subset \bar{X}$ we have $Y_{SE} \subset Y_{bd}$, i.e., the target images belongs to the boundary of the convex hull of the image set. Without loss of generality, we refer to the structure of a biobjective frontier ($p = 2$). Each nondominated facet of Y_{bd} may be treated as the hypotenuse of a right triangle (the other legs are parallel to the axes). The supported set Y_{SE} then decomposes Y into triangular regions which together contain the entire nondominated frontier. However, inside of one such triangle, *any number* of unsupported nondominated images may exist. While the images from $Y - Y_{SE}$ must exist in these triangular regions (otherwise, $\tilde{D}(\bar{X})$ would be contradicted), there is *no guarantee* that the images are *nondominated.* For instance, suppose for some $C \in \tilde{D}(\bar{X})$, a solution from $x \in \mathcal{X} - \bar{X}$ dominates $x' \in \bar{X} - \bar{X}_{SE}$. This dominance relationship does not interfere with stability of $C\bar{X}$, and hence $C \in D^*_{SE}(\bar{X}_{SE}) \cap \tilde{D}(\bar{X})$ is still possible while $C \notin D^*_E(\bar{X}, \bar{X}_{SE})$. Furthermore, the solution x could even be efficient within this triangle, and as long as it remains unsupported, we would still have $C \in D^*_{SE}(\bar{X}_{SE}) \cap \tilde{D}(\bar{X})$ while $C \notin D^*_E(\bar{X}, \bar{X}_{SE})$. Hence both cases are proven. □

Example 1.10. *We revisit Example 1, wherewhere $\bar{X} = \bar{X}_{SE} = \{x^1, x^2\} = \{(0, 6), (2, 5)\}$. Figure C.12 illustrates three sets introduced in this study, which are outlined in detail, subsequently.*

- *$\tilde{D}(\bar{X})$ is in blue, and gives a loose outer approximation which is both symmetric over $\theta_2 = \theta_1$ and $\theta_2 = \theta_1 \pm \pi$ lines. It also includes all self-collinear objective matrices.*
- *$D^*_{SE}(\bar{X}_{SE})$ is in red, and in this instance is a strictly better outer approximation than $\tilde{D}(\bar{X})$.*

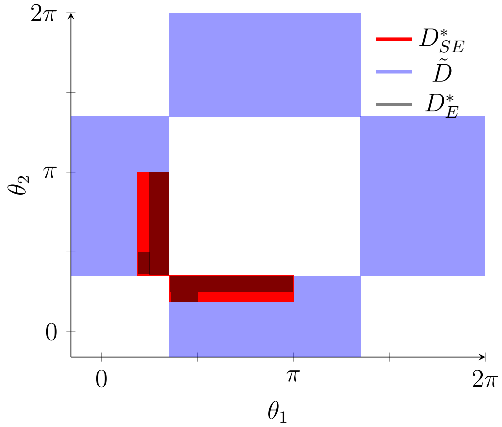

Figure C.12: Illustrated characterization gap $D^*_{SE} \cap \tilde{D} - D^*_E$. The outer approximation $D^*_{SE} \cap \tilde{D}$ is too large because it contains objective matrices which allows for a third (unsupported) efficient solution.

- $D^*_E(\bar{X}, \bar{X}_{SE})$ *is in dark gray. It excludes inverse infeasible objective matrices from* $D^*_{SE}(\bar{X}_{SE})$ *for which feasible solution* $(1, 5) \in \mathcal{X}$ *becomes an unsupported efficient solution. Note that the existence of unsupported efficient solutions does not occur in single-objective contexts, and the challenge for the multiobjective inverse problem remains open.*

$\tilde{D}(\bar{X})$. Note that $x^2 - x^1 = [+2, -1]$, whose polar transformation yields $\theta = \tan^{-1}(-1/2) \approx -0.46$ radians. Therefore, the square

$$S^1 = [-0.46 - \pi/2, -0.46 + \pi/2] \times [-0.46 - \pi/2, -0.46 + \pi/2]$$

contains all objective matrices where x^2 dominates x^1 (modulo 2π). Now, $x^1 - x^2 = [-2, +1]$ is antiparallel, so its polar transformation yields $\theta = \pi + \tan^{-1}(-1/2) \approx 2.67$. The square

$$S^2 = [2.67 - \pi/2, 2.67 + \pi/2] \times [2.67 - \pi/2, 2.67 + \pi/2]$$

contains all objective matrices where x^2 dominates x^1 (modulo 2π). Hence, the set difference provides $\tilde{D}(\bar{X}) = \mathbb{R}^2 - S^1 - S^2$. In Figure C.12, set $\tilde{D}(\bar{X})$ is indicated by blue, S^1 is the four outer white boxes (duplicated due to periodicity), and S^2 is the central white box.

$D^*_{SE}(\bar{X}_{SE})$. First, suppose x^1 is optimal for c^1, and x^2 is optimal for c^2. Then, c^1 must be chosen from the cone bounded by vectors $[-1, 0]$ and $[1, 2]$, so $\theta^1 \in [1.107, \pi]$. Also, c^2 must be chosen from the cone bounded by vectors $[1, 2]$ and $[3, 2]$, so $\theta^2 \in [0.588, 1.107]$. So the rectangle

$$[1.107, \pi] \times [0.588, 1.107]$$

contains all objective matrices where x^i is optimal for c^i, where $i \in \{1, 2\}$. By reversing or mirroring these intervals, we have that rectangle

$$[0.588, 1.107] \times [1.107, \pi]$$

contains all objective matrices where x^{3-i} is optimal for c^i, where $i \in \{1, 2\}$.

References

[1] S. Chakraborty, R. D. Raut, T. Rofin, S. Chakraborty, A comprehensive and systematic review of multi-criteria decision-making methods and applications in healthcare, Healthcare Analytics (2023) 100232.

[2] M. Ehrgott, Ç. Güler, H. W. Hamacher, L. Shao, Mathematical optimization in intensity modulated radiation therapy, Annals of Operations Research 175 (1) (2010) 309–365.

[3] J. Andersson, A survey of multiobjective optimization in engineering design, Department of Mechanical Engineering, Linktjping University. Sweden (2000) 1–34.

[4] R. T. Marler, J. S. Arora, Survey of multi-objective optimization methods for engineering, Structural and Multidisciplinary Optimization 26 (2004) 369–395.

[5] M. Ehrgott, Multicriteria Optimization, Springer Science & Business Media, 2005.

[6] M. Ehrgott, X. Gandibleux, Multiobjective combinatorial optimization—theory, methodology, and applications, Multiple Criteria Optimization: State of the Art Annotated Bibliographic Surveys (2002) 369–444.

[7] D. White, A bibliography on the applications of mathematical programming multiple-objective methods, Journal of the Operational Research Society 41 (8) (1990) 669–691.

[8] H. W. Hamacher, K.-H. Küfer, Inverse radiation therapy planning—a multiple objective optimization approach, Discrete Applied Mathematics 118 (1-2) (2002) 145–161.

[9] O. Tavaslıoğlu, T. Lee, S. Valeva, A. J. Schaefer, On the structure of the inverse-feasible region of a linear program, Operations Research Letters 46 (1) (2018) 147–152.

[10] A. J. Schaefer, Inverse integer programming, Optimization Letters 3 (4) (2009) 483–489.

[11] S. Fallah, T. K. Ralphs, N. L. Boland, On the relationship between the value function and the efficient frontier of a mixed integer linear optimization problem, Mathematical Methods of Operations Research 100 (1) (2024) 175–220.

[12] A. Dunbar, S. Sinha, A. J. Schaefer, Relaxations and duality for multiobjective integer programming, Mathematical Programming 207 (1) (2024) 577–616.

[13] A. Tarantola, Inverse problems: methods for data fitting and model parameter estimation (1987).

[14] D. Burton, P. L. Toint, On an instance of the inverse shortest paths problem, Mathematical Programming 53 (1992) 45–61.

[15] R. K. Ahuja, J. B. Orlin, Inverse optimization, Operations Research 49 (5) (2001) 771–783.

[16] T. C. Chan, N. Kaw, Inverse optimization for the recovery of constraint parameters, European Journal of Operational Research 282 (2) (2020) 415–427.

[17] K. Ghobadi, H. Mahmoudzadeh, Inferring linear feasible regions using inverse optimization, European Journal of Operational Research 290 (3) (2021) 829–843.

[18] G. Iyengar, W. Kang, Inverse conic programming with applications, Operations Research Letters 33 (3) (2005) 319–330.

[19] J. Zhang, C. Xu, Inverse optimization for linearly constrained convex separable programming problems, European Journal of Operational Research 200 (3) (2010) 671–679.

[20] J. Zhang, L. Zhang, An augmented Lagrangian method for a class of inverse quadratic programming problems, Applied Mathematics and Optimization 61 (1) (2010) 57.

[21] Z. Erkin, M. D. Bailey, L. M. Maillart, A. J. Schaefer, M. S. Roberts, Eliciting patients' revealed preferences: An inverse Markov decision process approach, Decision Analysis 7 (4) (2010) 358–365.

[22] Z. Ghatrani, A. Ghate, Inverse Markov decision processes with unknown transition probabilities, IISE Transactions 55 (6) (2023) 588–601.

[23] Z. Duan, L. Wang, Heuristic algorithms for the inverse mixed integer linear programming problem, Journal of Global Optimization 51 (2011) 463–471.

[24] J. B. Lamperski, A. J. Schaefer, A polyhedral characterization of the inverse-feasible region of a mixed-integer program, Operations Research Letters 43 (6) (2015) 575–578.

[25] L. Wang, Cutting plane algorithms for the inverse mixed integer linear programming problem, Operations Research Letters 37 (2) (2009) 114–116.

[26] T. C. Chan, R. Mahmood, I. Y. Zhu, Inverse optimization: Theory and applications, Operations Research (2023).

[27] T. Lee, M. Hammad, T. C. Chan, T. Craig, M. B. Sharpe, Predicting objective function weights from patient anatomy in prostate IMRT treatment planning, Medical Physics 40 (12) (2013) 121706.

[28] T. C. Chan, T. Craig, T. Lee, M. B. Sharpe, Generalized inverse multiobjective optimization with application to cancer therapy, Operations Research 62 (3) (2014) 680–695.

[29] J. J. Boutilier, T. Lee, T. Craig, M. B. Sharpe, T. C. Chan, Models for predicting objective function weights in prostate cancer IMRT, Medical Physics 42 (4) (2015) 1586–1595.

[30] M. Naghavi, A. A. Foroughi, M. Zarepisheh, Inverse optimization for multi-objective linear programming, Optimization Letters 13 (2) (2019) 281–294.

[31] J. Roland, Y. D. Smet, J. R. Figueira, On the calculation of stability radius for multi-objective combinatorial optimization problems by inverse optimization, 4OR 10 (4) (2012) 379–389.

[32] A. Przybylski, X. Gandibleux, M. Ehrgott, A recursive algorithm for finding all nondominated extreme points in the outcome set of a multi-objective integer programme, INFORMS Journal on Computing 22 (3) (2010) 371–386.

[33] S. Helfrich, T. Perini, P. Halffmann, N. Boland, S. Ruzika, Analysis of the weighted Tchebycheff weight set decomposition for multiobjective discrete optimization problems, Journal of Global Optimization 86 (2) (2023) 417–440.

[34] H. M. Wagner, Global sensitivity analysis, Operations Research 43 (6) (1995) 948–969.

References

[1] Leslie Lamport, *LaTeX: a document preparation system*, Addison Wesley, Massachusetts, 2nd edition, 1994.